Communication

Influence of Intra-granular Ferrite on the Tensile Behavior of Intercritically Annealed 12 pct Mn TWIP+TRIP Steel

SANGWON LEE and BRUNO C. DE COOMAN

The influence of intra-granular ferrite islands, fully embedded in austenite matrix grains, on the tensile behavior of intercritically annealed Fe-12 pct Mn-0.3 pctC-3 pctAl TWIP + TRIP steel was investigated. The presence of intra-granular ferrite, which nucleated at twin boundaries during annealing, resulted in an increased yield strength by the Orowan dislocation looping mechanism and the generation of geometrically necessary dislocations at the ferrite particle/austenite matrix interface. The intra-granular ferrite also induced the formation of secondary twin variants. The resulting twin–twin intersections nucleated additional α'-martensite, thereby leading to an enhanced TRIP effect.

The high-manganese twinning-induced plasticity (TWIP) steels have been widely studied because of their superior combination of strength and ductility due to the dynamic Hall–Petch effect caused by mechanical twinning.[1–3] The relatively low yield strength of about 400 MPa of fully austenitic TWIP steel compared to conventional advanced high-strength steel has been recognized early on as a major limitation in applications where ultra-high strength is required.[4] Yield strength enhancement of TWIP steel is currently achieved by strain hardening. This is done by cold-rolling recrystallization-annealed TWIP steel.

The present contribution shows that the recently developed intercritically annealed high Mn multi-phase $(\alpha + \gamma)$ steels offer an alternative approach to the conventional fully austenitic 15 to 22 pct Mn TWIP steel.[5–7] These multi-phase steels exhibit a high yield strength (>500 MPa) and a ductility comparable to the conventional high Mn TWIP steel.

SANGWON LEE, Graduate Student, is with the Graduate Institute of Ferrous Metallurgy, Pohang University of Science and Technology, Pohang 790-784, South Korea. BRUNO C. DE COOMAN, Professor, is with the Graduate Institute of Ferrous Metallurgy, Pohang University of Science and Technology, and also Director, with the Materials Design Laboratory, Pohang University of Science and Technology. Contact e-mail: decooman@postech.ac.kr
Manuscript submitted July 10, 2014.
Article published online January 6, 2015.

The steel design is based on the nucleation of small ferrite islands fully embedded in austenite grains. Intra-granular ferrite has been reported to nucleate in austenite grains on Ti_2O_3 oxide inclusions in low-carbon steel,[8] MnS-V(C,N) precipitates in Fe-Mn-C alloys,[9] (Ti,V)(C,N) precipitates in high Ti-bearing steel,[10] and CuS-MnS particles in medium C micro-alloyed steel.[11] Imandoust et al.[12] reported that the intra-granular ferrite nucleated at austenite twin boundaries during compression tests of TWIP steels carried out at 473 K (200 °C). In the present work, inter-granular ferrite was formed during the intercritical annealing of cold-rolled Fe-12 pctMn-0.3 pctC-3 pctAl steel containing mechanical twins and deformation-induced martensite.

The inter-granular ferrite has a higher hardness than austenite due to solid solution hardening.[7] The austenite grain size decreases with increasing ferrite volume fraction.[5] The combination of the hard ferrite phase and the austenite grain refinement effectively increases the yield strength. In addition, the austenite stability is increased with increasing ferrite volume fraction due to the partitioning of C and Mn to the intercritical austenite.

For the present study, an intercritical annealing procedure was used to form small intra-granular ferrite islands fully embedded in austenite grains. The tensile properties were then compared to those obtained after a recrystallization annealing in the full austenite stability range. The microstructural characterization revealed the clear influence of the intra-granular ferrite islands on the dislocation density evolution and the plasticity-enhancing deformation mechanisms in Fe-12 pctMn-0.3 pctC-3 pctAl steel.

The chemical composition of the steel used in present study was Fe-12 pctMn-0.3 pctC-3 pctAl, in mass percentage. The steel was produced by vacuum induction melting and hot rolled. The hot-rolled microstructure was austenitic with less than 2 vol pct of inter-granular ferrite as shown in Figure 1(a). No athermal martensite was present in the hot-rolled microstructure. Hot-rolled sheets were cold rolled to a thickness of 1.25 mm, corresponding to a 50 pct reduction. Figure 1(b) shows that both mechanical twins and deformation-induced martensite were formed during cold rolling. Cold-rolled sheets were annealed in the temperature range of 423 K to 923 K (150 °C to 650 °C) to form different volume fractions of intra-granular ferrite. The heating rate was +4 K/s. The samples were held at the annealing temperature for 3600 seconds prior to cooling to room temperature using a cooling rate of −30 K/s.

The annealing temperature dependence of the sum of the volume fractions of martensite and ferrite, as measured by means of magnetic saturation, is shown in Figure 2(a). The sum of the volume fractions of martensite and ferrite at room temperature decreased slightly with increasing annealing temperature from 423 K to 523 K (150 °C to 250 °C) due to the reverse martensite-to-austenite transformation. The sum of the volume fractions of martensite and ferrite then increased due to the austenite-to-ferrite transformation in temperature range of 523 K to 673 K (250 °C to 400 °C), as the austenite transformed to martensite upon cooling to
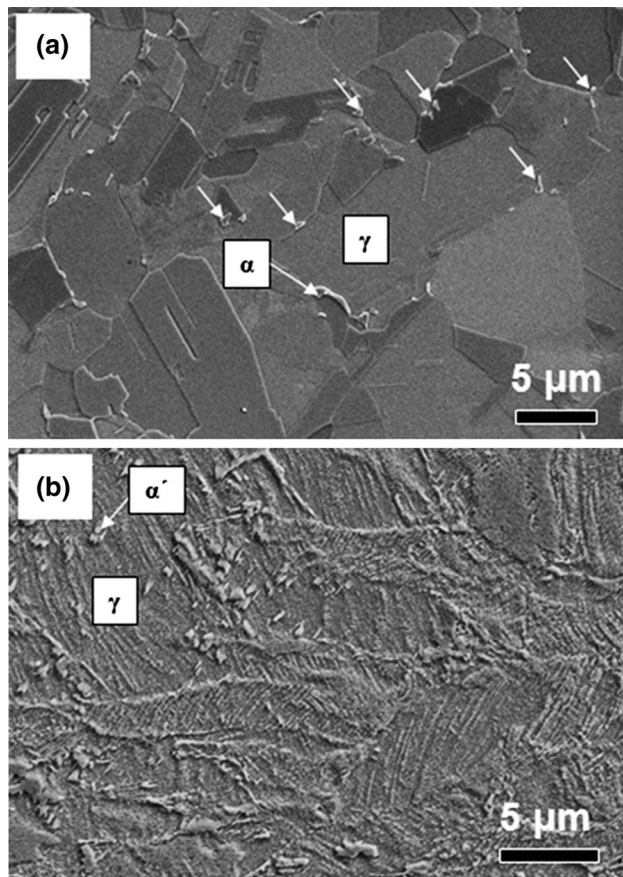
Fig. 1—SEM micrographs of (a) hot-rolled and (b) cold-rolled Fe-12 pctMn-0.3 pctC-3 pctAl steel.

room temperature. For annealing temperatures higher than 673 K (400 °C), the sum of the volume fractions of martensite and ferrite decreased due to the decrease of the ferrite fraction to its equilibrium value. The ferrite fraction was obtained by subtracting the martensite fraction from the experimentally measured sum of the volume fractions of martensite and ferrite. The highest ferrite volume fraction was obtained after annealing at 773 K (500 °C).

Figures 2(b) through (d) show the three annealing cycles used to investigate the influence of the intra-granular ferrite islands on the mechanical properties of Fe-12 pctMn-0.3 pctC-3 pctAl steel. In annealing cycle 1 of Figure 2(b), cold-rolled samples were heated to 1023 K (750 °C) and held at this temperature for 600 seconds. In annealing cycle 2 of Figure 2(c), an additional aging at 773 K (500 °C) was used to form intra-granular ferrite, prior to heating to 1023 K (750 °C) and cooling to room temperature. In the annealing cycle 3 of Figure 2(d), the additional aging at 773 K (500 °C) was used to form intra-granular ferrite, prior to cooling to room temperature.

ASTEM-E8 sub-size tensile samples (gage length: 25 mm, gage width: 6.25 mm) with tensile axis aligned along the rolling direction were tested at room temperature with a strain rate of 10^{-3} s^{-1} in a ZWICK universal tensile testing machine. The fraction of strain-induced martensite was monitored during the tensile tests by means of a portable ferrite analyzer.

The samples were carefully polished with a 1200-grit paper and subsequently electro-polished in a 95 pct CH_3COOH + 5 pct $HClO_4$ solution to remove any strain-induced martensite formed during the mechanical polishing. The microstructures of the samples were observed by means of a ZEISS ULTRA-55 field emission scanning electron microscope (FE-SEM). The deformation mechanisms were characterized using a JEOL JEM-2010F UHR field emission transmission electron microscope (FE-TEM). The samples for TEM observation were chemically thinned to a thickness less than 100 μm in a 95 pct H_2O_2 + 5 pct HF solution prior to electro-polishing in a 95 pctCH_3COOH + 5 pct $HClO_4$ solution.

Energy dispersive spectroscopy (EDS) was used to charaterize the composition of the strain-induced martensite and the intra-granular ferrite, as the C and Mn partitioned from ferrite to austenite during intercritical annealing. The partitioning reduced the Mn content of the ferrite to 6 to 7 wt pct, while the martensite contained 12 pct Mn.

Figure 3 shows the microstructure of Fe-12 pctMn-0.3 pctC-3 pctAl steel after the three annealing cycles. Figure 3(a) shows a fully austenitic microstructure after annealing cycle 1 of Figure 2(b). Figure 3(b) shows a microstructure consisting of austenite and intra-granular ferrite after the annealing cycle 2 of Figure 2(c). The austenite grain size was approximately 2.5 μm after both annealing cycles. The grain size of the intra-granular ferrite was in the range of 40 to 300 nm. Figure 3(c) shows a high volume fraction of ferrite nucleated at twin boundaries in the microstructure obtained after the annealing cycle as shown in Figure 2(d). The mechanical twins are still present in the microstructure as they are thermally stable at 773 K (500 °C). This is similar to the observation made by Bouaziz et al.[13] that a high density of mechanical twins was present in a cold-rolled Fe-22 pctMn-0.6 pctC TWIP steel after annealing at 773 K (500 °C) for 3600 seconds. As mechanical twin boundaries acts as strong obstacles to glide dislocation motion, their presence results in a high density of dislocation pile-ups near twin boundaries. This appears to facilitate the nucleation of ferrite along twin boundaries. Annealing at 1023 K (750 °C) results in full recrystallization and the removal of the mechanical twins. At this temperature, the ferrite islands formed at the twin boundaries become embedded in the austenite grains as intra-granular ferrite islands. The inter-granular ferrite is less effectively nucleated at the austenite
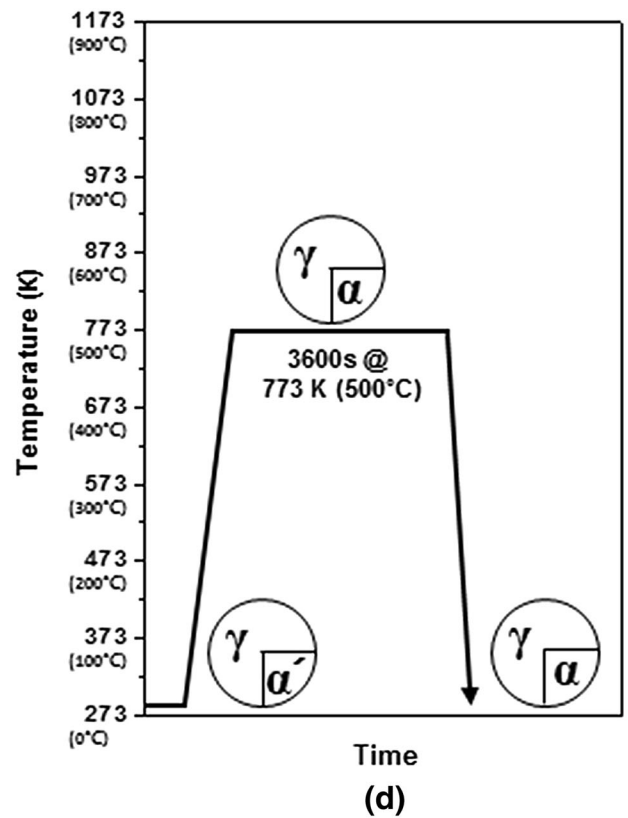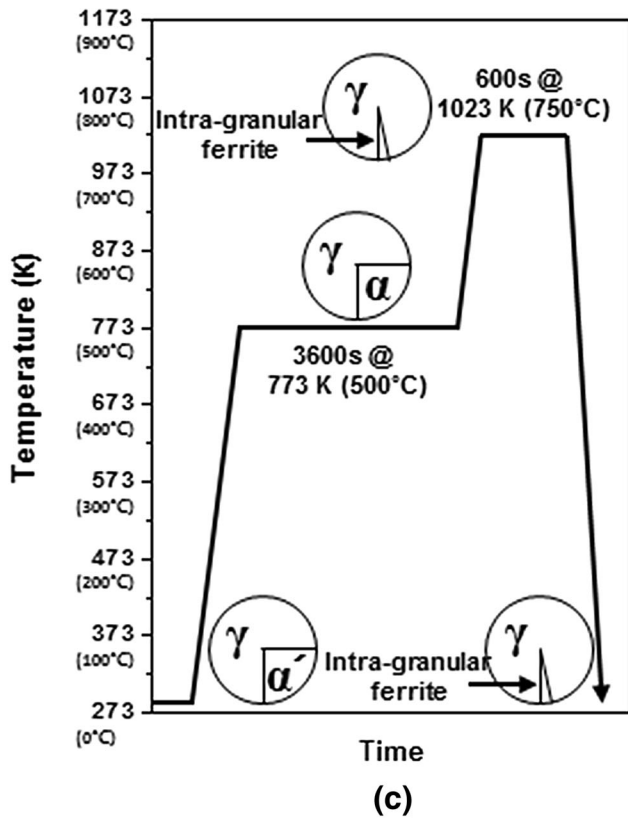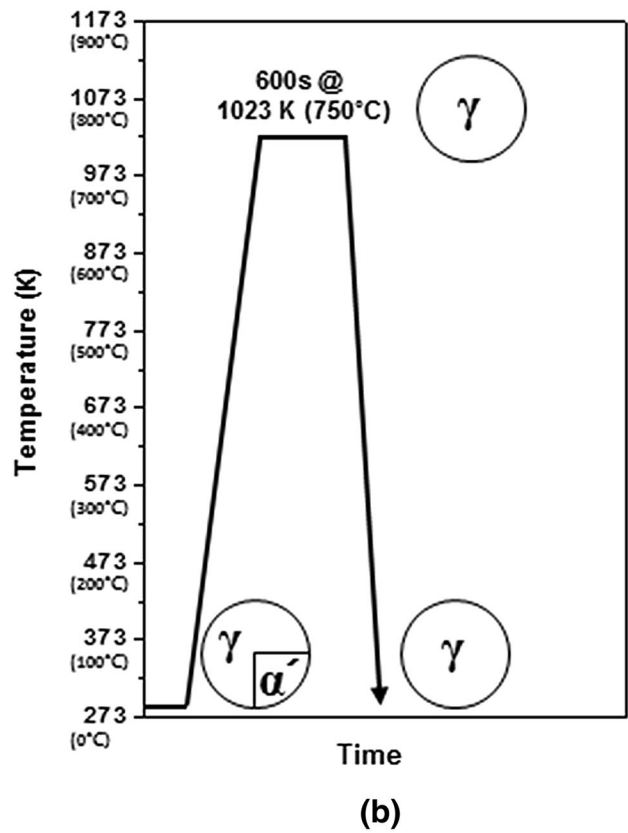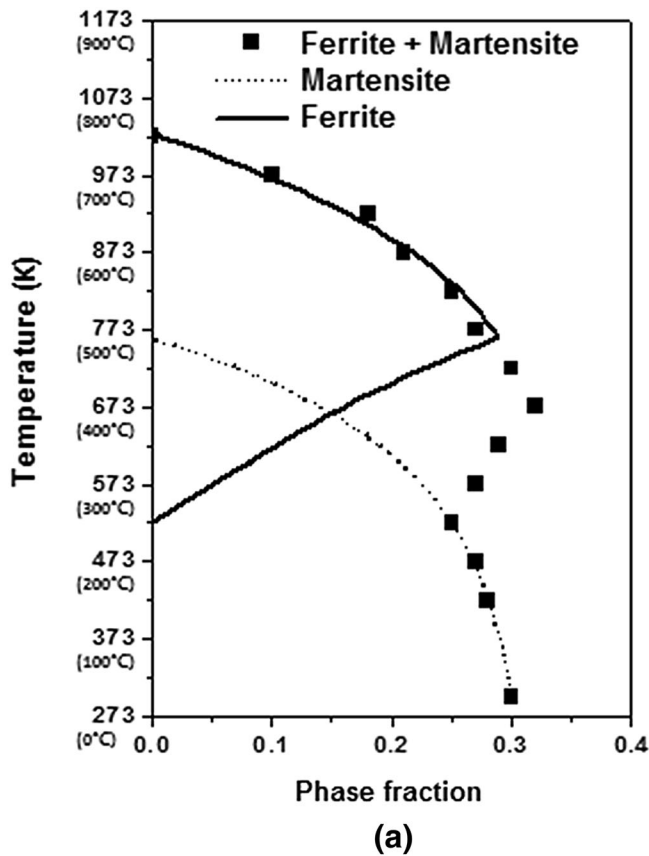
Fig. 2—(a) Annealing temperature dependence of the ferrite and martensite phase fractions. Schematic diagrams showing the three annealing cycles used in the present study: (b) cycle 1, (c) cycle 2, and (d) cycle 3.
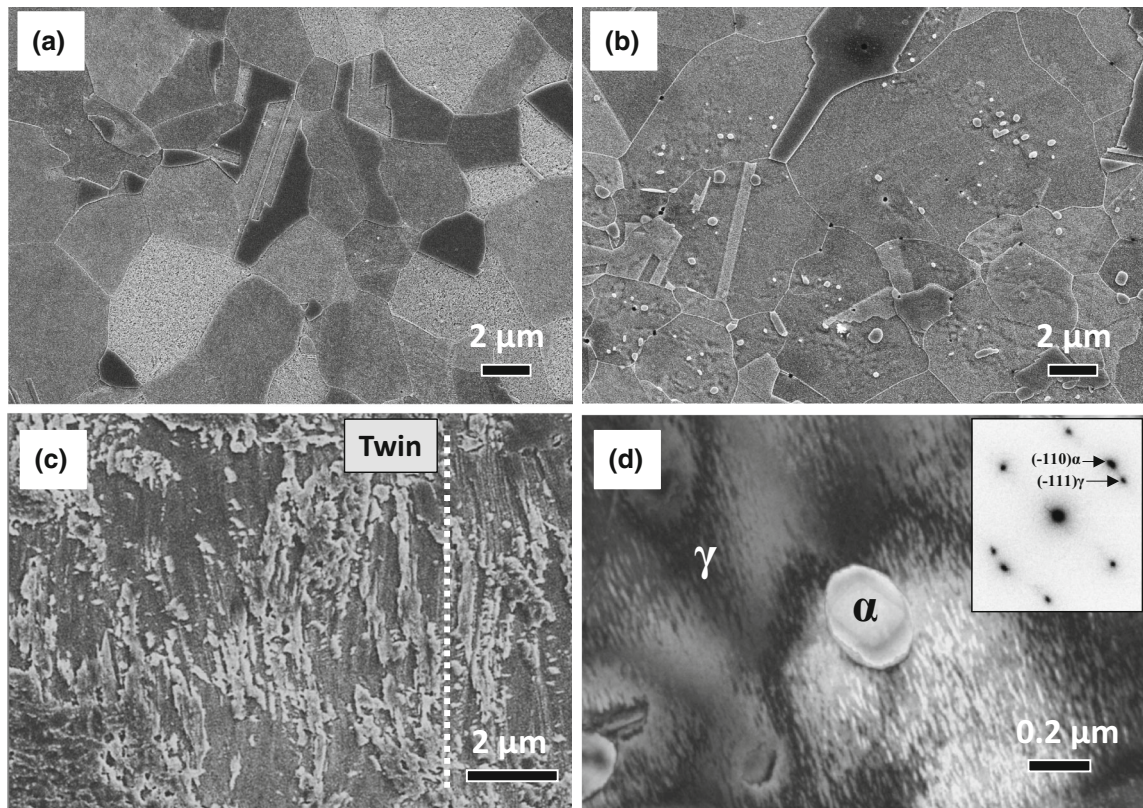
Fig. 3—(*a*) SEM micrograph of the Fe-12 pctMn-0.3 pctC-3 pctAl steel after annealing cycle 1, (*b*) cycle 2, and (*c*) cycle 3. (*d*) Bright-field TEM micrograph of Fe-12 pctMn-0.3 pctC-3 pctAl steel annealed according to cycle 2, with the corresponding selected area diffraction (SAD) patterns for the austenite matrix and the embedded ferrite island after cycle 2. The electron beam is parallel to a $\langle 011 \rangle_\gamma$ direction.

grain boundaries. The TEM micrographs of Figure 3(d) show an intra-granular ferrite island embedded in an austenite grain and the corresponding selected area diffraction pattern. The Nishiyama–Wasserman orientation relationships between austenite and intra-granular ferrite island, *i.e.*, $\{111\}\gamma$ // $\{110\}\alpha$, $\langle 0\text{-}11 \rangle \gamma$ // $\langle 001 \rangle \alpha$, were observed. The intra-granular ferrite islands were equiaxed, with smoothly curved interphase boundaries.

Figure 4(a) shows the comparison of tensile test results for Fe-12 pctMn-0.3 pctC-3 pctAl steel with a fully austenitic microstructure and with a microstructure containing intra-granular ferrite. The microstructure containing intra-granular ferrite had a higher yield strength and a larger total elongation. The work hardening rate was similar for both annealing cycles, as shown in Figure 4(b).

The tensile behavior of intercritically annealed multi-phase Fe-12 pctMn-0.3 pctC-3 pctAl steel resulted from the fact that two plasticity-enhancing strain hardening mechanisms, the TWIP effect and the TRIP effect, occured in succession. The fraction of strain-induced

martensite was monitored during the tensile tests by means of a portable ferrite analyzer. The results are shown in Figure 4(c). The strain-induced martensite transformation kinetics of both samples were similar up to a strain of 28 pct, at which point the fully austenitic sample fractured. The martensite transformation occurring in the intercritically annealed sample allowed for much larger strains and a fracture at 46 pct.

The deformation mechanisms in Fe-12 pctMn-0.3 pctC-3 pctAl steel with a fully austenitic microstructure and with a microstructure containing intra-granular ferrite in the austenite grains are compared in Figure 5. The deformation in intercritically annealed Fe-12 pctMn-0.3 pctC-3 pctAl steel was controlled by the TWIP and TRIP plasticity-enhancing mechanisms which occured in succession. Similar mechanical properties controlled by the same combination of plasticity-enhancing mechanisms were previously reported for intercritically annealed multi-phase Fe-10 pctMn-0.3 pctC-3 pctAl-2 pctSi steel.[5] In this steel, the martensite nucleated at the intersection of mechanical twins
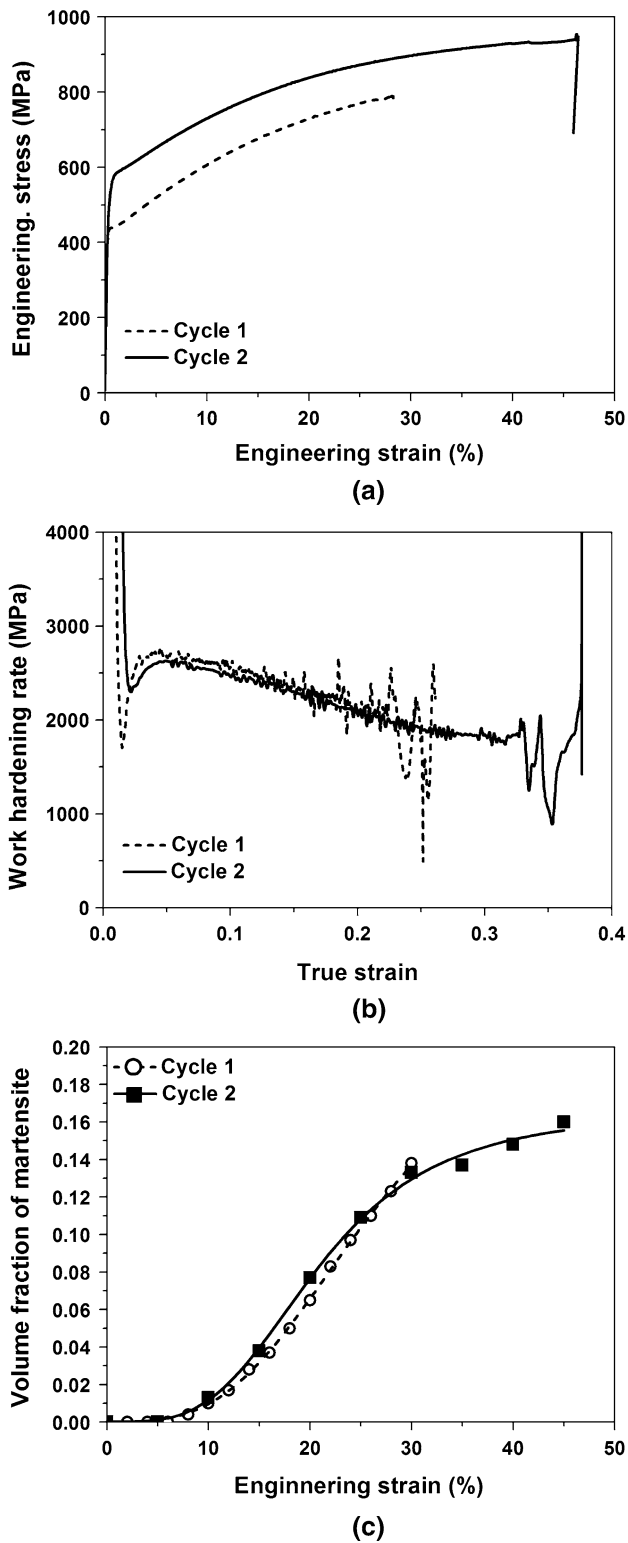
(a)

(b)

(c)

Fig. 4—Annealing cycle dependence of the tensile properties of Fe-12 pctMn-0.3 pctC-3 pctAl steel: (*a*) Engineering stress–strain curves. (*b*) Work hardening rate. (*c*) Volume fraction of strain-induced martensite as a function of strain.

formed in the austenite grains during straining. Figures 5(a) through (c) show clearly that this deformation mechanism was also activated in the intercritically annealed Fe-12 pctMn-0.3 pctC-3 pctAl steel. The martensite volume fraction increased with increasing strain as shown in Figures 5(d) through (f).

The presence of the intra-granular ferrite islands resulted in an additional effect, illustrated in Figures 5(g) through (k). At low strain (Figure 5(g)), the dislocations in the austenite are seen to bow out between intra-granular ferrite islands. This indicates that the ferrite islands acted as Orowan-type precipitates relative to the glide dislocations in the austenite grains. As the strain increased beyond 20 pct, twins belonging to a twin variant T_2 different from the primary twin variant T_1 were emitted from the austenite/ferrite island boundaries as shown in Figure 5(h). These secondary twins induced additional twin–twin intersections, which are the main nucleation sites for strain-induced martensite. Figures 5(i) through (k) show evidence for the martensite transformation between two intra-granular ferrite islands.

The intra-granular ferrite contributed to strengthening by (a) the Orowan dislocation looping mechanism and (b) the generation of a high density of geometrically necessary dislocations. The smaller inter-granular ferrite particles acted as hard impenetrable obstacles which strengthen the austenite matrix by the Orowan dislocation looping mechanism. In addition, the strain gradient between the larger hard ferrite particles and the softer austenite matrix resulted in the formation of a high density of geometrically necessary dislocations. This additional accumulation of dislocations, due to the presence of the inter-granular ferrite, enhanced the TWIP and TRIP effects,[14] thereby contributing to a higher total elongation as compared to the fully austenitic steel. Although the additional volume fraction of martensite was relatively small, the strain hardening caused by the additional martensite transformation resulted in a pronounced increase of the total elongation to 46 pct.

In summary, the effect of intra-granular ferrite islands fully embedded in austenite grains on the tensile behavior of intercritically annealed Fe-12 pctMn-0.3 pctC-3 pctAl steel was investigated. The intra-granular ferrite islands were nucleated at austenite twin boundaries during intercritical annealing. The intra-granular ferrite islands were shown to act as Orowan-type obstacles to glide dislocation, leading to an increase of the flow stress. The intra-granular ferrite induced additional intersections of mechanical twins, thereby enhancing the TRIP effect by increasing the nucleation of martensite. Both effects contributed to the substantial strength-ductility balance (*i.e.,* the product of ultimate tensile strength and total elongation) of intercritically annealed Fe-12 pctMn-0.3 pctC-3 pctAl steel of 44,000 MPa pct.
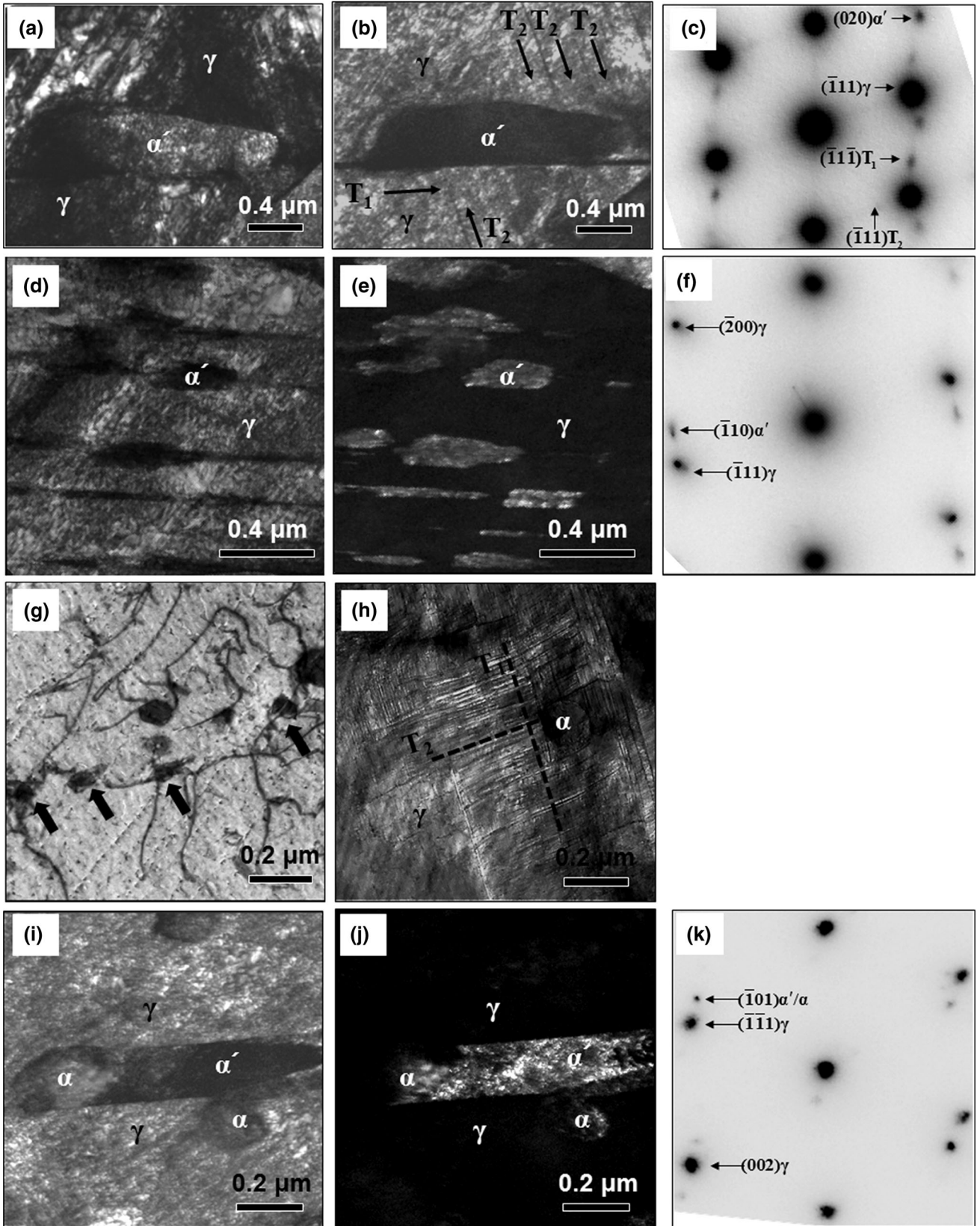
◀ Fig. 5—(*a*) Bright-field TEM micrograph of the microstructure of Fe-12 pctMn-0.3 pctC-3 pctAl strained to 15 pct after annealing cycle 1. (*b*) Corresponding dark-field micrograph for austenite. (*c*) Corresponding selected area diffraction pattern. The electron beam parallel was to a $\langle 011 \rangle_\gamma$ direction. (*d*) Bright-field TEM micrograph of the microstructure of Fe-12 pctMn-0.3 pctC-3 pctAl strained to 20 pct after annealing cycle 1. (*e*) Corresponding dark-field micrograph of martensite. (*f*) Corresponding selected area diffraction pattern. The electron beam was parallel to a $\langle 011 \rangle_\gamma$ direction. (*g*) STEM image of the Fe-12 pctMn-0.3 pctC-3 pctAl, annealed according to cycle 2, strained to 2 pct and to (*h*) 20 pct. (*i*) Bright-field TEM micrograph of martensite and ferrite in Fe-12 pctMn-0.3 pctC-3 pctAl annealed according to cycle 2 and strained to 25%. (*j*) Corresponding dark-field micrograph of the martensite. (*k*) Corresponding selected area diffraction pattern with the electron beam parallel to a $\langle 011 \rangle_\gamma$ direction.

REFERENCES

1. T. Dieudonné, L. Marchetti, M. Wery, J. Chêne, C. Allely, P. Cugy, and C.P. Scott: *Corr. Sci.*, 2014, vol. 82, pp. 218–26.
2. F. Reyes-Calderôn, I. Mejia, A. Boulaajaj, and J.M. Cabrera: *Mater. Sci. Eng. A*, 2013, vol. 560, pp. 552–60.
3. O. Bouaziz and N. Guelton: *Mater. Sci. Eng. A*, 2001, vols. 319–321, pp. 246–49.
4. J.-E. Jin and Y.-K. Lee: *Acta Mater.*, 2012, vol. 60, pp. 1680–88.
5. S.W. Lee and B.C. De Cooman: *Metall. Mater. Trans. A*, 2014, vol. 45A, pp. 709–16.
6. V. Torabinejad, A. Zarei-Hanzaki, S. Moemeni, and A. Imandoust: *Mater. Des.*, 2011, vol. 32, pp. 5015–21.
7. S.W. Hwang, J.H. Ji, E.G. Lee, and K.-T. Park: *Mater. Sci. Eng. A*, 2011, vol. 528, pp. 5196–5203.
8. J.-H. Shim, Y.W. Cho, S.H. Chung, J.-D. Shim, and D.N. Lee: *Acta Mater.*, 1999, vol. 47, pp. 2751–60.
9. T. Furuhara, T. Shinyoshi, G. Miyamoto, J. Yamaguchi, N. Sugita, N. Kimura, N. Takemura, and T. Maki: *ISIJ Int.*, 2003, vol. 43, pp. 2028–37.
10. J. Hu, L.X. Du, and J.J. Wang: *Scripta Mater.*, 2013, vol. 68, pp. 953–56.
11. I Madariaga and I Gutiérrez: *Acta Mater.*, 1999, vol. 47, pp. 951–60.
12. A. Imandoust, A. Zarei-Hanzaki, and H.R. Abedi: *Scripta Mater.*, 2012, vol. 67, pp. 995–98.
13. O. Bouaziz, S. Allain, C.P. Scott, P. Cugy, and D. Barbier: *Curr. Opin. Solid State Mater. Sci.*, 2011, vol. 15, pp. 141–68.
14. R. Song, D. Ponge, and D. Raabe: *Scripta Mater.*, 2005, vol. 52, pp. 1075–80.